ground-state C_2HF. Fluorination appears to have little effect upon the predicted ΔE for isomerization from unsaturated carbene to alkyne. The ZPVE corrected value of $\Delta E = \sim 44$ kcal mol^{-1} for C_2HF is about 1 kcal mol^{-1} larger than the value reported for the unfluorinated system. Stabilization of the transition state for 1,2-hydrogen migration by fluorination is apparent in a slight ($\sim$1 kcal mol^{-1}) lowering of the classical barrier height to 2.4 kcal mol^{-1}. A very small activation energy for hydrogen migration ($\sim$0.8 kcal mol^{-1}) is predicted after a correction for differences in zero-point vibrational energies has been made.

Optimized geometries, harmonic vibrational frequencies, and relative energies have also been predicted for $\tilde{X}\ ^2A'$ fluorovinylidene anion and two low-lying excited states ($^3A'$ and $^3A''$) of neutral fluorovinylidene. The 10a′ MO is singly-occupied in each of these three states. The adiabatic electron affinity of fluorovinylidene predicted here [EA(HFC=C:) = 1.62 eV] is in excellent agreement with the experimentally reported[21] value of EA(HFC=C:) = 1.718 eV. Note that EA(HFC=C:) is more than 1.2 eV *larger* than the experimentally reported[20] value for vinylidene [EA(H_2C=C:) = 0.49 eV]. This indicates that fluorination has stabilized the anion relative to the neutral ground state. Furthermore, the $^3A'$ and $^3A''$ excited states of neutral fluorovinylidene are much lower-lying ($\sim$0.8 eV) than the corresponding $\tilde{a}\ ^3B_2$ and $\tilde{b}\ ^3A_2$ excited states of vinylidene.[21] A close examination of SCF molecular orbital eigenvalues for $\tilde{X}\ ^1A'$ fluorovinylidene and $\tilde{X}\ ^1A_1$ vinylidene reveals that the HFC=C: 10a′ LUMO lies lower in energy than the corresponding H_2C=C: $2b_2$ LUMO. This suggests that electronic states of fluorovinylidene with the 10a′ MO singly-occupied should lie lower in energy than the corresponding states of vinylidene with the $2b_2$ MO singly-occupied.

The $^3A'$ and $^3A''$ excited states of fluorovinylidene are predicted to be nearly isoenergetic [$\Delta T_0(^3A'' - {}^3A') = +0.12$ eV]. Recall that the $^3A'$ state arises from the LUMO ← SHOMO excitation and the $^3A''$ state arises from the LUMO ← HOMO excitation. The SCF molecular orbital eigenvalues for the fluorovinylidene 2a″ HOMO and the vinylidene $1b_1$ HOMO show that fluorination does not significantly alter the energy of the CC π-bonding orbital. However, the 9a′ HFC=C: carbene lone-pair SHOMO lies *lower* in energy than the analogous $5a_1$ H_2C=C: carbene lone-pair SHOMO. This suggests that the $^3A'$ and $^3A''$ states of fluorovinylidene should lie *closer* in energy than the corresponding $\tilde{a}\ ^3B_2$ and $\tilde{b}\ ^3A_2$ states of vinylidene because fluorination has made the LUMO ← SHOMO excitation less favorable.

Acknowledgment. This research was supported by the U.S. Department of Energy, Office of Basic Energy Sciences, Division of Chemical Sciences, Fundamental Interactions Branch, Grant No. DE-FG09-87ER13811. This material is based upon work supported under a National Science Foundation Graduate Fellowship. The authors would like to thank Mary Gilles and Prof. W. C. Lineberger for providing the results of their negative ion photoelectron spectroscopy experiments prior to publication. Dr. Yukio Yamaguchi, George Vacek, and J. Russell Thomas deserve thanks for helpful discussions and thorough proofreading during the preparation of this manuscript. We would also like to thank Dr. Gustavo E. Scuseria for the CCSD(T) codes[41,42] used in this research.

Bonding and Dynamics of the $ThCr_2Si_2$ and $CaBe_2Ge_2$ Type Main Group Solids: A Monte Carlo Simulation Study

Chong Zheng

Contribution from the Department of Chemistry, Northern Illinois University, DeKalb, Illinois 60115. *Received March 6, 1992*

Abstract: A Monte Carlo simulation study based on the extended-Hückel tight-binding method was carried out to examine the thermodynamic properties of the $ThCr_2Si_2$ and $CaBe_2Ge_2$ type main group solids. At room temperature, the $ThCr_2Si_2$ structure is more stable owing to a less dispersed filled band and a lower Fermi level. Weaker bonding also counts for the larger atomic thermal motion in layers D of the $CaBe_2Ge_2$ structure. At higher temperatures, the entropic contribution will become more important and thus can favor the $CaBe_2Ge_2$ type. The free-energy difference at room temperature between these structures was calculated using the free-energy perturbation technique. The calculations indicate that the $ThCr_2Si_2$ type has not only lower energy, but also lower free energy. At high temperatures, however, the $CaBe_2Ge_2$ type can be the more stable structure.

Introduction

The $ThCr_2Si_2$ type family comprises more than 400 compounds.[1] It has attracted much attention because many of the solids show a variety of novel physical properties, such as superconductivity,[2] unique magnetic behavior, valence fluctuation, and heavy fermion phenomenon.[3] Some of these members also have intriguing chemical and structural properties. For example, they can transform from the $ThCr_2Si_2$ type to the closely related $CaBe_2Ge_2$ structure at a temperature range of 1000–1700 °C.

(1) (a) Marchand, R.; Jeitschko, W. *J. Solid State Chem.* **1978**, *24*, 351. (b) Jeitschko, W.; Jaberg, B. *J. Solid State Chem.* **1980**, *35*, 312. (c) Hofmann, W. K.; Jeitschko, W. *J. Solid State Chem.* **1984**, *51*, 152. (d) Parthé, E.; Chabot, B.; Braun, H. F.; Engel, N. *Acta Crystallogr., Sect. B: Struct. Sci.* **1983**, *39*, 588. (e) Pearson, W. B. *J. Solid State Chem.* **1985**, *56*, 278. (f) Hulliger, F. *Helv. Phys. Acta* **1985**, *58*, 216.

(2) (a) Shelton, R. N.; Braun, H. F.; Musik, E. *Solid State Commun.* **1984**, *52*, 797. (b) Braun, H. F. *J. Less-Common Met.* **1984**, *100*, 105.

(3) (a) Steglich, F.; Aarts, J.; Bredl, C. D.; Lieke, W.; Meschede, D.; Franz, W.; Schäfer, H. *Phys. Rev. Lett.* **1979**, *43*, 1892. (b) Lieke, W.; Rauchschwalbe, U.; Bredl, C. D.; Steglich, F.; Aarts, J.; de Boer, F. R. *J. Appl. Phys.* **1982**, *53*, 2111. (c) Assmus, W.; Herrmann, M.; Rauchschwalbe, U.; Regel, S.; Lieke, W.; Spille, H.; Horn, S.; Weber, G.; Steglich, F.; Cordier, G. *Phys. Rev. Lett.* **1984**, *52*, 469. (d) Stewart, G. R. *Rev. Mod. Phys.* **1984**, *56*, 755. (e) Varma, C. M. *Comments Solid State Phys.* **1985**, *11*, 221. (f) Fulde, P.; Keller, J.; Zwicknagl, G. *Solid State Phys.* **1988**, *41*, 2. (g) *Theory of Heavy Fermions and Valence Fluctuations*: Kasuya, T., Saso, T., Eds.; Springer-Verlag: New York, 1985. (h) Schlottmann, P. *Phys. Rep.* **1989**, *181*, 1. (i) Reehuis, M.; Jeitschko, W. *J. Phys. Chem. Solids* **1990**, *51*, 961. (j) Das, I.; Sampathkumaran, E. V.; Vijayaraghavan, R. *J. Less-Common Met.* **1991**, *171*, L13.

0002-7863/93/1515-1047$04.00/0

The room-temperature $CaBe_2Ge_2$ type can be obtained by quenching from high temperatures.[4] Substitution of certain elements can also lead to the switching of the structural types.[5]

The two structural types are shown in **1** and **2**. The $ThCr_2Si_2$ structure consists of only one type of layer, which we call layer A. The $CaBe_2Ge_2$ structure, however, is built up with alternating A and D layers (see **3** and **4**). In layer A, the more electropositive

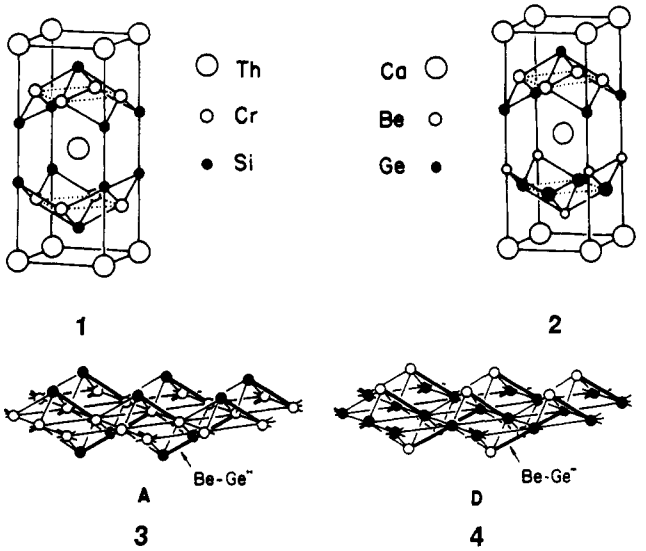

element (such as Be) occupies the center lattice sites, whereas, in D, the more electronegative element (Ge) resides at the center sites. Because the orbital overlap between the center sites is larger than that between the outer sites, there is more band dispersion for the center sites. Using the correlation between orbital overlap and band dispersion, one can conceptually build up qualitative band structure of the layers from the Be–Ge dimers.

The orbitals of the Be–Ge dimer are divided into an upper block, which is mostly of the more electropositive Be character, and a lower block, which is mostly Ge orbitals. The lower block is almost filled with electrons because the formal electron count of $Ca^{2+}(Be_2Ge_2)^{2-}$ gives a negatively charged dimer $Be–Ge^-$ with seven electrons in the lower four orbitals. The bonding pattern is that of a typical polar diatomic.

When the layers are built from the dimers, the orbitals develop into bands. To construct layer A, one needs to put the Be end of the dimer into the center lattice sites. Because of the larger orbital overlap which we stated above, this results in a larger dispersion in the upper block, the Be band, which is empty. Conversely, in D, there is larger dispersion in the lower block, which is almost filled. Thus layer D has a higher Fermi level (ϵ_F) and is energetically less stable than layer A. The schematic interaction diagram is illustrated in **5**. The D-A interlayer

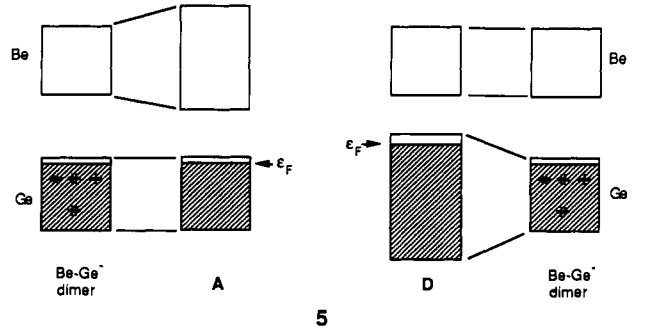

donor–acceptor type interaction, however, is more favorable than the A–A interaction. The balance between the intralayer and interlayer interactions can be fine-tuned by the substitution of elements with different electronegativities and orbital overlap capabilities. Thus for some combinations of elements, the $CaBe_2Ge_2$ structure can be more stable. The bonding properties of these compounds have been analyzed in detail in terms of energy bands in the solid state.[6]

The mechanistic and thermodynamic aspect of the transformation from the low-temperature allotrope to the high-temperature one, nevertheless, is not very well understood. In this contribution, we use a Monte Carlo simulation method based on the extended-Hückel tight-binding method to study the thermodynamic properties, particularly the temperature dependence of free energies, of these compounds. Among our objectives is an understanding of why the $CaBe_2Ge_2$ structure can be more stable than the $ThCr_2Si_2$ type at high temperatures.

Methods

The extended-Hückel type tight-binding method,[7] in conjunction with the Metropolis Monte Carlo scheme,[8a,b] was used in the simulations. Although the extended-Hückel Hamiltonian can describe the angular dependence of solid-state interactions reasonably well, it usually has difficulties in optimizing bond distances. Thus we add two terms to the extended-Hückel Hamiltonian. The total Hamiltonian used in our simulations is

$$H = H_{EH} + \sum_{i,j}\left(\frac{q_i q_j}{r_{ij}} + \frac{A_{ij}}{r_{ij}^{12}} - \frac{B_{ij}}{r_{ij}^{6}}\right)$$

where H_{EH} is the extended-Hückel Hamiltonian. The extended-Hückel energy is calculated by diagonalizing the H_{EH} matrix in each Monte Carlo step. The extended-Hückel parameters and the choice of special k points are summarized in the Appendix. The second term represents Coulomb and Lennard-Jones interactions. The Coulomb term is calculated using the Ewald sum method because, in general, the sum is only conditionally convergent. In this method, the summation is such that each point charge is surrounded by a charge distribution of equal magnitude and opposite sign, which spreads out radially. When the summation is Fourier-transformed into reciprocal space, it has a simple form that can be easily coded into a computer program. The formalism we used is due to de Leeuw et al. and Heyes.[8c,10a] We tested the convergence and chose to use a 100-wave-vector summation in the reciprocal lattice space and the damping parameter $\kappa = 5/L$, where L is the lattice constant. The Lennard-Jones interaction is summed over atom pairs within 18 Å. The atomic charges were calculated based on a Mulliken population analysis in each Monte Carlo step. The Lennard-Jones parameters were derived by assuming a 0.5-eV potential constant in combination with the equilibrium interatomic distance in the actual crystal structure. The numeric values of these parameters are listed in the Appendix. The modification of the extended-Hückel Hamiltonian with the addition of the second term was pioneered by Anderson, who has showed that much improvement can be obtained in reproducing experimental values of lattice constants, atomization energies, and bulk moduli of simple covalent solids.[8d] Wang et al. have also demonstrated that the Si phonon spectral density and bulk moduli calculated with a similar extended-Hückel method are in good agreement with experimental and first-principle calculation results.[8e] Recently, the extended-Hückel method in conjunction with simulated annealing implementation in Hoffmann's

(4) (a) Braun, H. F.; Engel, N. Parthé, E. *Phys. Rev. B* **1983**, *28*, 1389. (b) Higashi, I.; Lejay, P.; Chevalier, B.; Étourneau, J.; Hagenmuller, P. *Rev. Chim. Miner.* **1984**, *21*, 239.

(5) (a) Eisenmann, B.; Schäfer, H. Z. Anorg. *Allg.* Chem. **1974**, *403*, 163. (b) Cordier, G.; Dörsam, G.; Röhr, C. *J. Less-Common Met.* **1990**, *166*, 115. (c) Lux, C.; Wenski, G.; Mewis, A. Z. *Naturforsch.* **1991**, *B46*, 1035.

(6) (a) Zheng, C.; Hoffmann, R. *J. Am. Chem. Soc.* **1986**, *108*, 3078. (b) Zheng, C.; Hoffmann, R. *Z. Naturforsch., B* **1986**, *41B*, 292. (c) Hoffmann, R.; Zheng, C. *J. Phys. Chem.* **1985**, *89*, 4175. (d) Zheng, C.; Hoffmann: R.; Nesper, R.; von Schnering, H.-G. *J. Am. Chem. Soc.* **1986**, *108*, 1876.

(7) Hoffmann, R. J. *Chem. Phys.* **1963**, *39*, 1397. Hoffmann, R.; Lipscomb, W. N. *J. Chem. Phys.* **1962**, *36*, 2179; **1962**, *37*, 2872. Ammeter, J. H.; Bürgi, H.-B.; Thibeault, J. C.; Hoffmann, R. *J. Am. Chem. Soc.* **1978**, *100*, 3686. Whangbo, M.-H.; Hoffmann, R.; Woodward, R. B. *Proc. R. Soc. London* **1979**, *A366*, 23.

(8) (a) *Applications of the Monte Carlo Method in Statistical Physics*; Binder, K., Ed.; Springer-Verlag: New York, 1984. (b) *Monte Carlo Methods in Statistical Physics*, 2nd ed.; Binder, K., Ed.; Springer-Verlag: New York, 1986. (c) de Leeuw, S. W.; Perram, J. W.; Smith, E. R. *Proc. R. Soc. London* **1980**, *A373*, 27. Heyes, D. M. *J. Chem. Phys.* **1981**, *74*, 1924. (d) Anderson, A. B. *J. Chem. Phys.* **1975**, *162*, 1187. Nath, K.; Anderson, A. B. *Solid State* Commun. **1988**, *66*, 277. Anderson, A. B.; Nichols, J. A. *J. Am. Chem. Soc.* **1986**, *108*, 1385. (e) Wang, C. Z.; Chan, C. T.; Ho, K. M. *Phys. Rev. B* **1989**, *39*, 8586. (f) Wong, Y.-T.; Schubert, B.; Hoffmann, R. *J. Am. Chem. Soc.* **1992**, *114*, 2367.

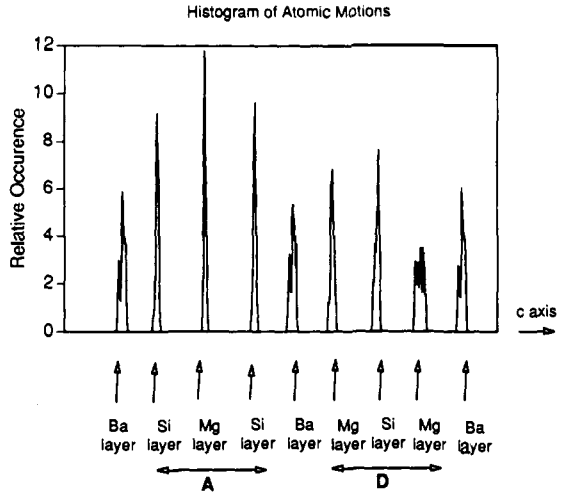

Figure 1. Histogram of atomic motions in a 2000-step Monte Carlo simulation for the $CaBe_2Ge_2$ structure. The abscissa represents the z value along c axis for each layer of atoms.

group gave reasonably good geometry for Si(111) surface reconstruction.[8f] The simplicity and transparency of this method thus allow us to do simulations of more complicated solid-state structures of chemical interest.

A prototype $BaMg_2Si_2$ structure was used in our simulation study, because this structure has been well studied and shown to gradually transform from the $ThCr_2Si_2$ to the $CaBe_2Ge_2$ structure by elemental substitution, **6**.[5a] The cutoff distance of 18 Å corresponds to four cells

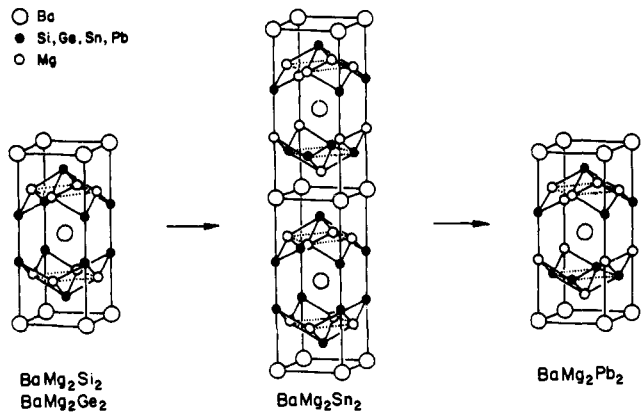

6

in the x–y direction and three cells in the z direction in the tetragonal structure. The tetragonal cell contains 10 atoms and corresponds to two unit cells in the $ThCr_2Si_2$ structure.

All atoms are moved randomly in each Monte Carlo step. The step size of atomic motion in the Metropolis scheme was adjusted at different temperatures such that the acceptance ratio is about 50%. Typically, it is about 0.04 Å at room temperature. The lattice vector lengths were allowed to move to mimic a constant-pressure condition, but the tetragonal symmetry was maintained during the simulations. All data collections were carried out after a minimal 1000-step equilibration. Although at room temperature the occupancy of bands higher than Fermi level is negligible, at higher temperatures it can be significant. Thus the occupancy of the bands was calculated according to Fermi–Dirac distribution $n = 1/[\exp\{(e - \epsilon_F)/k_BT\} + 1]$ (k_B is the Boltzmann constant and e the band energy). The simulations were carried out on the Cray Y-MP supercomputer at the National Center for Supercomputing Applications at the University of Illinois at Urbana—Champaign and on a Silicon Graphics 4D/310 GTX workstation at NIU.

Results and Discussions

The profile of the atomic motions of the $BaMg_2Si_2$ solid in the $CaBe_2Ge_2$ type structure at 300 K, viewed from the a–c side of the tetragonal cell (c axis, vertical in **1**, is now horizontal), is shown in Figure 1. It is the histogram of atomic motions in a 2000-step Monte Carlo simulation. As can be seen, the atomic motions in layer D, particularly those of Mg, are larger than in layer A, indicating weaker bonding in D.

Table I. Average Energy (eV) at 300 K from Monte Carlo Simulations[a]

	E_{total}	E_b	E_{nb}
$ThCr_2Si_2$ type	−414.7	−348.0	−66.7
$CaBe_2Ge_2$ type	−413.2	−347.5	−65.7

[a] E_{total} is the total energy. E_b the band energy, and E_{nb} the nonbonded energy, including Lennard-Jones and Coulomb energy. The average was calculated in a 2000-step Monte Carlo simulation.

This can be understood from the schematic bonding diagram **5**. In layer D, there is larger dispersion in the lower block of bonding character. Thus there is more antibonding character in this block. This antibonding feature is similar to the two-orbital–four-electron interaction for diatomic molecules.[15] Indeed, the overlap population between Mg and Si, shown in **7**, is smaller in

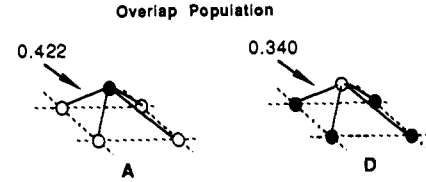

7

layer D than in layer A. The weaker bonding in layer D is therefore responsible for the larger thermal motions.

Because of the unfavorable bonding pattern, the calculated average band energy of the $CaBe_2Ge_2$ structure is higher than that of the $ThCr_2Si_2$ structure by about 0.5 eV for $BaMg_2Si_2$ (see Table I). The total energy, including the Coulomb and the Lennard-Jones contributions, is still higher for the $CaBe_2Ge_2$ by about 1.5 eV per unit cell. The energies at 300 K for these two structures are summarized in Table I.

The atomic displacement in both layers increases with temperature. In our simulation, the displacement becomes comparable to interatomic distance above 1400 K in layers D, and above 1500 K in both types of layers. Thus if Lindemann's theory of melting,[9] which states that the onset of melting occurs when atomic motion becomes comparable to interatomic distances, is applicable in these solids, then melting starts in layers D in the $CaBe_2Ge_2$ structure. The total energy for both structures also increases with temperature (see Figure 2), and the energy fluctuation becomes large above 1400 K for the $CaBe_2Ge_2$ structure.

The free energy difference can also be calculated, using the free energy perturbation method. In this method, the potential is parametrized with a parameter λ. When $\lambda = 0$, the Hamiltonian is that for the $ThCr_2Si_2$ structure, and when $\lambda = 1$, for the $CaBe_2Ge_2$ structure. In the extended-Hückel method, this is equivalent to parametrizing the Hamiltonian matrix elements as $H_{ij}(\lambda) = (1 - \lambda)H_{ij}(A) + \lambda H_{ij}(B)$, where $H_{ij}(A)$ and $H_{ij}(B)$ are the matrix elements for the $ThCr_2Si_2$ and the $CaBe_2Ge_2$ structures, respectively. λ is slowly changed from 0 to 1 such that the system is always at equilibrium.[10]

Because at any intermediate value of λ, the free energy $G(\lambda) = -\beta^{-1} \ln Q(\lambda)$, where $Q(\lambda) = \mathrm{Tr}\, e^{-\beta H(\lambda)}$ is the partition function, $\partial G(\lambda)/\partial\lambda = \mathrm{Tr}\,(\partial H/\partial\lambda\, e^{-\beta H(\lambda)})/\mathrm{Tr}\, e^{-\beta H(\lambda)} = \langle \partial H/\partial\lambda \rangle_\lambda$, which is the average value of $\partial H/\partial\lambda$ at the intermediate state λ. Thus the free energy difference is the integrated value of the average derivative of the Hamiltonian $H(\lambda)$ with respect to λ:

(9) See, for example: (a) Ubbelohde, A. R. *The Molten State of Matter, Melting and Crystal Structure*; Wiley: New York, 1978; Chapter 3. (b) Rosenberger, F. *Fundamentals of Crystal Growth I*; Springer-Verlag: New York, 1981.

(10) (a) Allen, M. P.; Tildesley, D. J. *Computer Simulation of Liquids*; Oxford University Press: New York, 1987; Chapter 7. (b) Brooks, C. L., III. *Int. J. Quantum Chem.* **1988**, *15*, 221. (c) Sussman, F.; Goodfellow, J. M.; Barnes, P.; Finney, J. L. *Chem. Phys. Lett.* **1985**, *113*, 221. (d) Brooks, C. L., III. *J. Phys. Chem.* **1986**, *90*, 6680. (e) McCammon, J. A.; Harvey, S. C. *Dynamics of Proteins and Nucleic Acids*; Cambridge University Press: New York, 1987. (f) Wong, C. F.; McCammon, J. A. *J. Am. Chem. Soc.* **1986**, *108*, 3830.

$$\Delta G = G(\lambda = 1) - G(\lambda = 0) = \int_0^1 \frac{\partial G}{\partial \lambda} d\lambda = \int_0^1 \left\langle \frac{\partial H(\lambda)}{\partial \lambda} \right\rangle_\lambda d\lambda$$

Using this method, we calculated the free energy difference to be 1.4 ± 1.0 eV from several 4000-step simulation runs with λ divided into 200 windows, favoring the $ThCr_2Si_2$ structure. The error in free energy was estimated by starting simulations with different initial conditions. The error is rather significant, probably because the change from one structure to another is not related by a martensitic transformation.[11] Thus equilibrium was not perfectly maintained during the simulations. Nevertheless, the free energy difference is not very different from the energy difference. This indicates that the entropic contribution is small at room temperature in favoring one of these two structures.

The free energy difference should change with temperature, however, and the entropic contribution may become important at higher temperatures. To study the temperature dependence of the free energy difference, we carried out a 6000-step simulation. During the simulation, the temperature is gradually increased from 300 K to 1400 K, divided into 200 window for averaging the total energy in each window. As we mentioned above, the step size of atomic motions was adjusted to maintain a 50% acceptance ratio in each window.

Since free energy is related to the canonical partition function $Q(T)$ through the equation $G(T) = -k_B T \ln Q(T)$, where $Q(T) = \mathrm{Tr}\, e^{-H/k_BT}$ is the partition function, calculated by taking the trace of e^{-H/k_BT}, the change of free energy with temperature can be calculated using the quantum mechanical version of the Gibbs–Helmholtz equation

$$\partial(G/T)/\partial(1/T) = \mathrm{Tr}\, He^{-H/k_BT} = \langle E \rangle_T$$

or its integrated form

$$\frac{G(T_2)}{T_2} - \frac{G(T_1)}{T_1} = \int_{T_1}^{T_2} \frac{-\langle E \rangle_T}{T^2} dT$$

where $\langle E \rangle_T$ is the average energy at temperature T.[12] The difference in temperature-scaled free energies ($g \equiv G/T$) between two structures can also be calculated, using the equation

$$\Delta\Delta g = \Delta g(T_2) - \Delta g(T_1) = \frac{\Delta G(T_2)}{T_2} - \frac{\Delta G(T_1)}{T_1} = \int_{T_1}^{T_2} -\frac{\langle \Delta E \rangle_T}{T^2} dT$$

where $\langle \Delta E \rangle_T$ is the averaged energy difference and $\Delta G(T)$ the free energy difference between the two structures at temperature T.

The above equation shows that if one structure always has higher average energy than the other in the temperature range T_1 to T_2 ($\langle \Delta E \rangle_T > 0$), then the temperature-scaled free energy difference, $\Delta\Delta g$, will become more and more negative. In other words, the structure with *higher* energy can have *lower* free energy at high enough temperature. In our case, the $CaBe_2Ge_2$ structure has higher average energy than the $ThCr_2Si_2$ type from 300 K to 1400 K (see Figure 2). Thus $\Delta\Delta g$ becomes more negative with increasing temperature (Figure 3). As can be seen in Figure 3, the contribution from the tight binding band energy is slightly more than half of the total contribution which includes band, Coulomb, and Lennard-Jones energies. This is a reflection of both the ionic and covalent characteristics of this type of solid which consist of covalent layered network and interstitial ions. If the initial free energy difference at 300 K ΔG_1 is 1.4 eV, or Δg_1 = 1.5/300 = 0.005 eV/K, then $\Delta\Delta g$ has to be less than −0.005 eV/K for ΔG_2 at higher temperature to be negative ($CaBe_2Ge_2$ more stable). As can be seen from Figure 3, this will only be possible above 1400 K at the extended-Hückel approximation level. If the initial free energy difference is 0.5 eV (Δg_1 = 0.0017 eV/K), this can happen below 1000 K. Because the calculated transition temperature is sensitive to the free energy difference at room temperature, one needs to be able to calculate the free energy

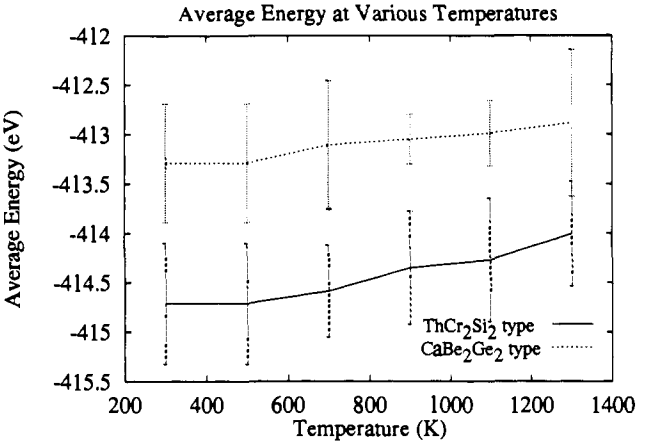

Figure 2. Average energy and fluctuation profile in as a function of temperature for both structures.

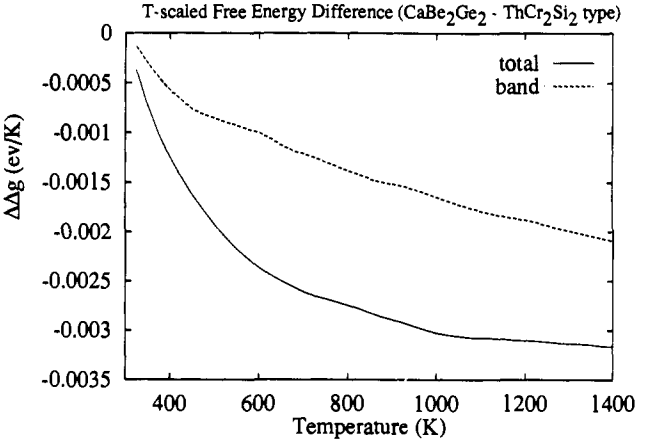

Figure 3. Temperature-scaled free energy difference $\Delta\Delta g$ as a function of temperature.

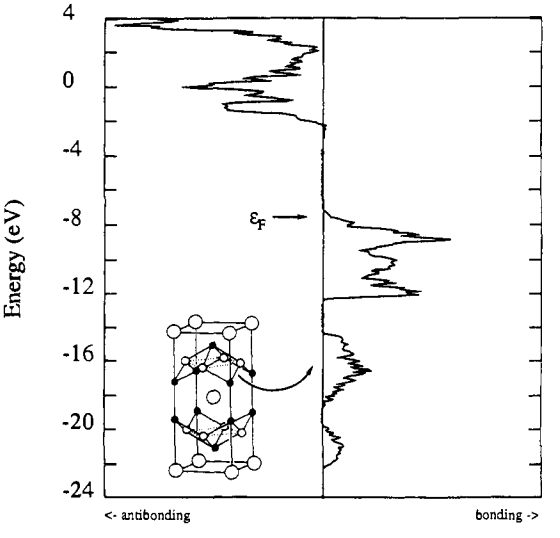

Figure 4. COOP curve for the Mg–Si bond in the $ThCrSi_2$ structure.

(11) West, A. R. *Solid State Chemistry and Its Applications*; Wiley: New York, 1984; pp 446.

(12) (a) Mark, A. E.; van Gunsteren, W. F.; Berendsen, H. J. C. *J. Chem. Phys.* **1991**, *94*, 3808. (b) Brooks, C. L., III *J. Phys. Chem.* **1986**, *90*, 6680. (c) Sussman, F.; Goodfellow, J. M.; Barnes, P.; Finney, J. L. *Chem. Phys. Lett.* **1985**, *113*, 373.

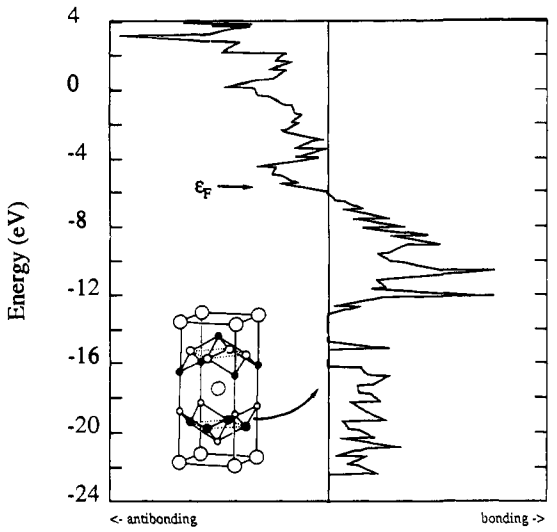

Figure 5. COOP curve for the Mg-Si bond in layer D of the $CaBe_2Ge_2$ structure.

Table II. Extended-Hückel Parameters

	orbital	H_{ii} (eV)	ζ
Ba	6s	-7.0	1.2
	6p	-4.0	1.2
Mg	3s	-9.0	1.2
	3p	-4.5	1.2
Si	3s	-17.3	1.38
	3p	-9.2	1.38

difference more accurately in order to predict the transition temperature.

Finally, one reason that the $CaBe_2Ge_2$ structure has higher average energy than the $ThCr_2Si_2$ type at higher temperatures is that its band gap is much smaller. Because of the larger band dispersion (see 5) in the $CaBe_2Ge_2$ structure, it is easier to for the electrons to be excited to the states above the Fermi level. This may lead to an additional contribution from vibronic excitations, as one referee pointed out. Figures 4 and 5 are the crystal orbital overlap population[13] (COOP) plots for the Mg-Si bonds in these two structures. These are really density of states weighted overlap populations, plotted in increasing energy, positive value indicating states contributing to bonding, and negative to antibonding. The magnitude shows how many states contribute to a bond, and how strong is the bond.

In Figures 4 and 5, one can see that the band gap is much larger for the $ThCr_2Si_2$ structure. Above the band gap, the states are all antibonding states. Thus if these states are occupied, the Mg-Si bond will be significantly weakened. This is the primary reason that at high temperatures, when these states are populated, the atomic fluctuation becomes greater. Because the band gap is larger, the antibonding states are populated at much higher temperatures for the $ThCr_2Si_2$ type structure.

Acknowledgment. This work has been supported in part by the National Science Foundation through the Presidential Young Investigator Program (CHE-91-57717) and by the Donors of the Petroleum Research Fund administered by the American Chemical Society. Part of the simulations were carried out on the Cray Y-MP supercomputer at the National Center for Supercomputing Applications at the University of Illinois at Urbana—Champaign.

Appendix

The extended-Hückel parameters used in the simulations are listed in Table II. The Lennard-Jones radii for atoms are taken from the $BaMg_2Si_2$ structure (a = 4.65 Å, c = 11.09 Å). The corresponding parameters for the atom pairs are: (A) Ba-Mg, 3.5114×10^6 eV Å^{12}; Ba-Si, 1.8092×10^6 eV Å^{12}; Mg-Si, 1.0654×10^5 eV Å^{12}; (B) Ba-Mg, 1.3250×10^3 eV Å^6; Ba-Si, 9.5110×10^2 eV Å^6; Mg-Si, 2.3080×10^2 eV Å^6. A set of 8K points generated using the method of Pack and Monkhorst[14] for tetragonal cell with lowest symmetry was used for the Monte Carlo simulations, and 64K points for the COOP calculations.

(13) (a) Wijeyesekera, S. D.; Hoffmann, R. *Organometallics* **1984**, *3*, 949. (b) Kertesz, M.; Hoffmann, R. *J. Am. Chem. Soc.* **1984**, *106*, 3453. (c) Saillard, J.-Y.; Hoffmann, R. *J. Am. Chem. Soc.* **1984**, *106*, 2006.
(14) Pack, J. D.; Monkhorst, H. J. *Phys. Rev. B* **1977**, *16*, 1748.
(15) Albright, T. A.; Burdett, J. K.; Whangbo, M.-H. *Orbital Interactions in Chemistry*; Wiley: New York, 1985; Chapter 2.

The Role of d Functions in Correlated Wave Functions: Main Group Molecules

Eric Magnusson

Contribution from the Department of Chemistry, University College, ADFA, University of New South Wales, Canberra ACT 2600, Australia. *Received March 11, 1992*

Abstract: Large d function contributions to Hartree-Fock wave functions of sulfur- and phosphorus-containing molecules are often cited as evidence for hypervalent spd hybridization and for violations of the octet rule. Recent work on hypercoordinate molecules invalidates this interpretation, but the possibility remains that hypervalent bonding may be facilitated by d orbital involvement in correlated wave functions. A large sample of molecules of the first- and second-row elements has been studied by electronic structure theory at correlated levels and the d function contributions compared with results obtained at the Hartree-Fock level. Whether molecules are hypercoordinate or not, d functions added to the basis set provide a fairly constant 52 kJ m^{-1} of the MP4 correlation extra energy per valence shell electron pair. d functions in the MP4 correction to Hartree-Fock wave functions neither polarize the wave function nor act as valence d "orbitals". They are correlating functions, their effects are largely atom-centered, and their major role is to provide angular correlation. By contrast, supplementary d functions in the Hartree-Fock part of the wave function are polarizing functions, the effects of which are concentrated in the overlap regions. d functions in these two roles provide a computationally convenient way to remove the restrictions of the small-basis Hartree-Fock model, but neither is consistent with the idea of a valence role for d orbitals in main group molecules or of an expanded octet.

Supplementary d functions are indispensable in electronic structure calculations of main group molecules for reproducing experimental quantities such as geometries, reaction energies, stretching frequencies, and deformation densities.[1] For example,

0002-7863/93/1515-1051$04.00/0